

# The NaNO<sub>3</sub>–KNO<sub>3</sub> phase diagram

R. Benages-Vilau<sup>a\*</sup>, T. Calvet<sup>a</sup>, M.A. Cuevas-Diarte<sup>a</sup> and H.A.J. Oonk<sup>b</sup>

<sup>a</sup>Departament de Cristal·lografia, Mineralogia i Dipòsits Minerals, Facultat de Geologia,  
Universitat de Barcelona (UB), Barcelona, Spain; <sup>b</sup>Department of Earth Sciences, Utrecht  
University, Utrecht, The Netherlands

\*Corresponding author. Email: rbenages@irec.cat

21 **ABSTRACT**

22 Many papers have been published in relation to the NaNO<sub>3</sub> -KNO<sub>3</sub> phase diagram  
23 determination in the last 160 years. These papers fall in two categories: (1) the solid-liquid  
24 equilibrium is assumed to be of the eutectic type, and (2) the solid-liquid equilibrium is  
25 considered as a loop with a minimum. The discordance between the two views is related to  
26 the slow transition kinetics that complicate the assessment of thermal ‘fluctuations’, and also  
27 to the appearance of a metastable form of potassium nitrate. The main result of this paper is  
28 the experimental phase diagram constructed with new experimental data so that we can  
29 assure that the second option is correct. This phase diagram is defined by a eutectoid  
30 invariant, an asymmetric immiscibility gap and a continuous solid solution with a minimum  
31 of melting point. Additionally, the Abu model simulates correctly the experimental piece of  
32 evidence.

33

34

35

36

## 37 1. INTRODUCTION

38 The first NaNO<sub>3</sub>-KNO<sub>3</sub> paper known was published in 1857.[1] Since then, many  
39 publications have appeared including a handbook.[2] A quick look at them permits us to  
40 make the following classification: (1) papers in which the solidliquid equilibrium is held for  
41 eutectic (limited subsolidus miscibility); and (2) papers in which it is represented by a loop  
42 with a minimum (evidence of complete subsolidus miscibility; continuous solid solution). In  
43 the older papers reviewed a eutectic system is proposed, followed by a continuous solid  
44 solution in the most recent literature,[1] while in the most recent publications, the notion of  
45 eutectic behaviour becomes prevalent again.[1,3-5] Thus, for more than 160 years, the  
46 following question has remained unanswered: Is the phase diagram described by eutectic  
47 behaviour or a melting point minimum? Phase diagram determination poses significant  
48 experimental difficulties as will be described in this paper and the solid-state region has been  
49 studied only partially - a complete thermodynamic explanation for the whole diagram is still  
50 to be published - which explains the lack of conclusive evidence on the topic. To describe a  
51 phase diagram, first we need to know the polymorphism of its components. An extensive  
52 summary of alkali nitrates polymorphism has been provided by Rao et al.[6] in 1975 and  
53 updated by Benages-Vilau et al. in a recent paper.[7] The main polymorphic characteristics  
54 of NaNO<sub>3</sub> and KNO<sub>3</sub> are described briefly in next paragraphs and schematically shown in  
55 Figure 1. The crystallographic parameter values are shown in Table 1.

56 Of relevant importance for this system are the phase transitions of the components.

57 (1) NaNO<sub>3</sub> shows a  $\lambda$  transition and it is discussed as a second-order phase transition  
58 (order-disorder) range of some 100 K.[9,10] In fact, it has been regarded as a  
59 particularly suitable system for testing certain theories and relations proposed for  
60 higher order transitions.[11] As far as we know, there are few reports in the  
61 literature that have considered these implications using differential scanning  
62 calorimetry (DSC) or other techniques. For example, Klement [12] was able to  
63 follow the transition until 10% of KNO<sub>3</sub> with DSC, while Ping et al. [5] were able  
64 to follow it until 50% of KNO<sub>3</sub>. However, they assigned two transitions for the  
65 equimolar composition, which has no thermodynamic significance. X-ray  
66 diffraction (XRD), which is the best technique to examine this gradual transition,  
67 was performed for NaNO<sub>3</sub> and/or CaCO<sub>3</sub> (isostructural compounds) by Antao and  
68 coworkers, [13,14] Ballirano [15] and Harris.[16]

69 Therefore, high temperature XRD (HTXRD) is mandatory to elucidate how this  
70 transition affects this phase diagram. We point out that some authors have missed  
71 its influence.[17,18]

72 (2) For KNO<sub>3</sub>, the metastable g-KNO<sub>3</sub> introduces some difficulties in the system. g-  
73 KNO<sub>3</sub> is observed when crystals are cooled from temperatures above 453 K, but it  
74 does not appear when crystals are heated from the a-form.[19] Nimmo and Lucas  
75 [20] found that the g-KNO<sub>3</sub> phase could be cooled to room temperature and remain  
76 stable for approximately 30 minutes. Furthermore, the stability of the g-KNO<sub>3</sub>  
77 phase depends on the manner of preparation, particle size, thermal history,  
78 impurities in the sample [21] and cooling rate.[22] Additionally, the hydrostatic  
79 stress may be responsible for the extended g-KNO<sub>3</sub> phase stability in small  
80 particles.[23] Some attempts to stabilize the g-phase at room temperature have been  
81 reported in the literature.[21,24-28] To close, Fermor and Kjekshus [29] highlight  
82 that when KNO<sub>3</sub> is heated at 468 K, it recrystallizes, a necessary step for the g-  
83 KNO<sub>3</sub> → b-KNO<sub>3</sub> transition on cooling.

84 The structural similarities of the different forms can be discussed paying attention to  
85 the possibility of forming solid solutions. First, let us remember the basic rules: two  
86 substances that form a continuous series of mixed crystals (solid solutions) have equal  
87 structure characteristics, and commensurable molar volumes. The notion of ‘equal structure  
88 characteristics’ comes down to equal space group and the same arrangement of the structural  
89 units. The notion of ‘commensurable molar volumes’ can be best illustrated with the help of  
90 a practical example of the alkali halides that have the NaCl type of structure. The two  
91 substances, NaCl and KCl, for which the molar volume of the former is 28% less than the  
92 one of the latter, are miscible in all proportions above 500 °C. The two substances, KI and  
93 RbI, with a difference in molar volume of 11%, mix in all proportions already at room  
94 temperature.[30]

95 Within the six possible combinations for the structure of the NaNO<sub>3</sub>-KNO<sub>3</sub> system,  
96 there is only one that fits the first requirement of having the same space group; b-KNO<sub>3</sub> and  
97 I-NaNO<sub>3</sub> have the same R3m space group and the same stacking sequence ABABAB...  
98 From the unit cell dimensions, ignoring any thermal expansion, it follows that the difference  
99 in molar volume is about 21%.

100 Another possibility is to find a g-KNO<sub>3</sub>-based solid solution because this phase is no  
101 substantially different from b-KNO<sub>3</sub>. [20,31] Consequently, one might expect a narrow  
102 degree of miscibility between I-NaNO<sub>3</sub> and g-KNO<sub>3</sub>. Furthermore, the introduction of  
103 sodium in the g-KNO<sub>3</sub> structure can, in certain ways, stabilize this hypothetical g-KNO<sub>3</sub>  
104 solid solution type. Some examples are found in the literature. [21,28,32]

105 For the determination of this phase diagram, the most used technique is thermal  
106 analysis (cooling and heating curves before the advent of the methods of differential  
107 microcalorimetry, such as DSC and differential thermal analysis (DTA)). [4,7,33-39] Some  
108 authors used the data from the second heating run [4,33,35,36] (generally these data are in  
109 line with a third heating run, which is seen as evidence for the system having arrived at  
110 equilibrium). This fact can introduce errors in the determination of the equilibrium phase  
111 diagram. In some of the early investigations, chemical analyses were carried out of  
112 coexisting solid and liquid phases, in order to determine the positions of solidus and liquidus.  
113 [40-43] Kofler, [44] who used a heating microscope, stated that it was very difficult to  
114 differentiate between the two components.

115 Regarding thermal analysis, it should be mentioned that the nitrates are highly  
116 corrosive salts - as shown in Ellingham diagrams [45] - therefore, the selection of the  
117 appropriate DSC capsule is an important topic. Decomposition products (mainly NO<sub>2</sub>) can  
118 react with aluminium, gold and platinum, particularly at high temperatures or during periods  
119 of prolonged exposure. [36,46-51]

120 Only four researchers have studied the mixed solid state by means of XRD. Kramer  
121 and Wilson [34] found rhombohedral NaNO<sub>3</sub> and orthorhombic KNO<sub>3</sub> patterns, when  
122 quenching both from above and below the liquidus line. They suggested that high  
123 temperature XRD is necessary to observe the solid solution. One year later, Kamimoto [35]  
124 worked with the equimolar composition using XRD at 473 K. He found a different XRD  
125 pattern and, in his opinion, a solid solution was formed. Unfortunately, he only gave stick  
126 patterns, which are difficult to interpret. He also observed the presence of g-KNO<sub>3</sub> upon  
127 cooling and although he did not recognize it as such, he pointed out that the sample was not  
128 in a thermodynamically stable state. Abe et al. [37] only observed immiscibility at room  
129 temperature. Zhang et al. [39] measured, by XRD, an equimolar mixture at 473 K and found  
130 a superposition of b-KNO<sub>3</sub> and I-NaNO<sub>3</sub> patterns. Additionally, Xu and Chen [32] argued

131 that XRD would give a structure with a level of symmetry higher than that measured by  
132 spectroscopic techniques in disordered systems.

133 In some papers, a calculated phase diagram is shown; it is either eutectic [4,39] or  
134 shows a solid-liquid loop with a minimum.[18,38] In 1990, Dessureault et al. [18] published  
135 a review of more than 30 papers. They conducted a statistical analysis of the thermodynamic  
136 data presented in these papers. They constructed a thermodynamic model for the system, and  
137 calculated a solid-liquid loop with a minimum. A very recent paper suggests the  
138 contrary,[52] they propose a eutectic-type phase diagram. However, careful reading of this  
139 paper indicates that the eutectic shape is imposed by the authors after reading the papers  
140 from Xu and Chen [32,52] and Berg and Kerridge.[3]

141 Another technique widely used in recent years is the Raman spectroscopy and all  
142 researchers who used it concluded that the NaNO<sub>3</sub>-KNO<sub>3</sub> phase diagram shows eutectic  
143 behaviour.[1,3,32,53] Mechanical characterization [54] and electrical measurements  
144 throughout the melting process [55,56] were also tried to address the problem.

145 Special attention must be given to the classical work by Tammann and Ruppelt  
146 published in 1931.[40] The two investigators applied the technique of cooling and heating  
147 curves, and completed their experiments with microscopic observations. They made two  
148 significant observations. First, crystals that had crystallized from the equimolar mixture had  
149 grown when kept at a 200 °C. According to the investigators, it is an evidence of the  
150 formation of a solid solution; a eutectic conglomerate would not do so. Second, the clear  
151 crystals that had crystallized from the melt became turbid on cooling at a given temperature  
152 as a function of composition. The onset temperature of turbidity was taken as the temperature  
153 at which the homogeneous sample enters the two-phase region. The minimum of the solid-  
154 liquid loop is about at 494 K and at the equimolar composition. The critical point of (solid-  
155 state) mixing, the top of the miscibility gap, is at about 448 K and between 40% and 50%  
156 KNO<sub>3</sub>.

157 Our group has extensive experience in polymorphism [30,57-60] and the phase  
158 diagram determination, [61,62] and our publications show the importance of using  
159 complementary techniques to effectively establish the stability regions within a binary  
160 system. From this position, we decided to study the NaNO<sub>3</sub>-KNO<sub>3</sub> system, in order to arrive  
161 at a conclusive answer to the true nature of the solid-liquid and solid-solid equilibrium. It is  
162 worth saying that in this paper XRD is the selected technique to characterize the equilibrium

163 state of different phase domains. Other complementary techniques, DSC, Raman and hot  
164 stage microscopy are used to check results obtained by XRD.

## 165 **Materials and methods**

166 High purity NaNO<sub>3</sub> and KNO<sub>3</sub> (99% or higher) were supplied by Quality  
167 Chemicals.[63] The purity of these nitrates was checked with inductively coupled plasma  
168 optical emission spectrometry (ICP-OES), revealing the impurities (in the ppm range) in  
169 NaNO<sub>3</sub> and KNO<sub>3</sub>, to be K<sup>+</sup> and Na<sup>+</sup>, respectively. Further purification was therefore not  
170 carried out. Water content in pure compounds was checked by thermogravimetry (being less  
171 than 0.3%).

172 Samples of 1 g of selected binary compositions (in total, there were 17 different  
173 samples, including pure compounds) were weighed in the correct molar proportions with an  
174 accuracy of 1 mg. They were melted and quenched inside a Pyrex glass tube in liquid  
175 nitrogen, then grounded and stored at room temperature.

176 Thermal analyses were performed with a Perkin Elmer DSC-7. We carried out many  
177 experiments to determine the most effective configuration. In this paper, we use aluminium  
178 capsules with holes, a sample weight of between 4.4 and 4.8 mg, a heating rate of 10 K/min  
179 and the upper temperature was approximately 10 K higher than the liquidus line for each  
180 composition. Working in this way, we have not noticed reaction between samples and  
181 aluminium capsules. Except for some samples, only two independent runs were carried out  
182 for each one of them. The DSC-7 was calibrated against indium and n-decane standards.  
183 From the DSC curve we have determined the onset temperature by extrapolation of the  
184 slopes and the ending temperature of the process by applying the shape factor, the enthalpy  
185 effects were evaluated integrating the DSC signals.[64] X-ray powder diffraction data was  
186 recorded with a Panalytical X'pert Pro diffractometer at room temperature with the Bragg-  
187 Brentano geometry ( $2\theta$ ). The pattern was acquired over a period of 39 minutes within a  
188 range of 4° to 100° ( $2\theta$ ) using Cu K $\alpha$ 1 radiation ( $\lambda$  1.5405 Å). Samples were mounted on  
189 a flat automatic sample charger. A spin rotation of 2 rev/min was selected to minimize the  
190 preferred orientation of the sample. The diffractometer was equipped with a hybrid  
191 monochromator and an X'Celerator detector. Temperature-dependent XRD was recorded  
192 with the same geometry for all compositions using an Anton Paar HTK-1200 N oven.  
193 Acquisition temperatures were set at 301-323-373-393-403-413-473-493-523-553-563-573-  
194 583-593K for a period of 2 h at each temperature. Stabilization time at each temperature was

195 5 minutes except at 393 K, which was 15 minutes to try achieving equilibrium. Additionally,  
196 a heating rate of 10 K/min was used and a maximum temperature depending on the sample  
197 melting point.

198 For selected compositions, in order to achieve equilibrium at high temperatures,  
199 annealing at various temperatures was carried out for up to 7 days in a FURCAP device from  
200 INEL diffractometer, which enables capillary samples to be heated from room temperature  
201 to 623 K. An X-ray powder diffraction pattern was collected after every 2 h of exposure.  
202 The sample is continuously rotated to minimize a preferred orientation. In this case, the  
203 diffraction patterns were recorded in a horizontally mounted 120° and 25 cm of radius curved  
204 position sensitive detector INEL CPS-120 in transmission geometry. The detector was used  
205 in its 4096 channels resolution mode. Samples were placed in 0.5 mm diameter glass  
206 Lindemann capillaries. Cu K $\alpha$ 1 radiation was selected by means of a Ge (111) primary flat  
207 monochromator. A parabolic multilayer mirror ‘OSMIC Gutman optics # 13B-413’ was  
208 placed between the tube and the monochromator. Na<sub>2</sub>Ca<sub>3</sub>Al<sub>2</sub>F<sub>14</sub> was used as an external  
209 standard to calibrate the detector and convert the channels to 2 $\theta$  values. The data were  
210 linearized to a constant step size of 0.029 in 2 $\theta$  by means of a cubic spline function.  
211 Calibration and linearization were performed with the PEAKOC application from  
212 DIFFRACTINEL software.

213 Materials Studio software was used for the cell parameter determination in some  
214 powder patterns,[65] while peak intensity and peak width were determined using the  
215 WinplotR software. Taking at least eight reflections of apparently well-separated peaks, the  
216 X-CELL indexing program [66] found the potential solutions of cell parameters and space  
217 groups. Those that best corresponded to the experimental XRD pattern were finally obtained  
218 using a Pawley profile-fitting procedure [67] available in the Powder Indexing module of  
219 Materials Studio.

220 A Raman spectroscopy study was carried out at room temperature with a Jobin Yvon  
221 T64000 Raman spectrometer. A liquid nitrogen cooled CCD detector was calibrated against  
222 TiO<sub>2</sub> and nominal laser power was 400 mW with a 514 nm wavelength. Five measurements  
223 of 10 sec each were performed from 24 to 1700 cm<sup>-1</sup>. Peak position and peak intensity were  
224 measured with the Origin Software.

225 For hot stage microscopic measurements, a Linkam THMSG-600 stage mounted to a  
226 Nikon Eclipse 50iPol Microscope was used. The sample was placed on a 7 mm quartz cover



227 slip, and encased within a pure silver lid so that it was heated from all sides, ensuring a  
228 uniform temperature. An LNP liquid nitrogen cooling system and a TMS94 temperature  
229 controller were used. Images were captured with a digital camera. In order to visualize the  
230 phase transition and the solidus line (on heating runs), a thin film was required. To obtain  
231 this, the sample was placed on a glass cover slip, heated above its melting point and then  
232 covered with another glass cover slip to obtain the thin film. The system was left for  
233 approximately 1 minute in the liquid state and was then finally cooled to room temperature  
234 at 100 K/min.

235

236

237

238

239

240

241

## 242 2. EXPERIMENTAL RESULTS

243 In this section, in a step-by-step manner, the results are presented of the experiments  
244 we carried out.

### 245 *DSC and hot stage microscopy experiments*

246 Generally, experiments by DSC provide information on the heat effect and the  
247 temperature characteristics of phase transitions. In our case, the experiments give  
248 information on (1) the eutectoid peak that goes together with the change of a-KNO<sub>3</sub> to b-  
249 KNO<sub>3</sub>; and (2) the change from solid to liquid.

250 The DSC measurements were reproducible in temperature and enthalpy values.  
251 Representative results obtained for the first heating run as a function of composition are  
252 gathered in Table 2. Thermal analysis normally is very valuable to detect the change between  
253 phase domains. Due to the characteristics of the phase diagram in this paper, it does not give  
254 accurate descriptions of these changes in the entire phase diagram. Furthermore, our  
255 measurements are pretty similar (in shape) to those of Ping et al.[5]

256 In order to detail the eutectoid change, compositions (with a 10% gap) were cycled  
257 two times. In the first heating run, we observed the eutectoid peak for all compositions at  
258 approximately 393 K. For the second heating run, the solid-solid transition was only  
259 observed in certain compositions; this may have some relation to the influence of the g-  
260 KNO<sub>3</sub> phase. To ascertain whether this was the case, some samples were recycled with a  
261 time lag (between either weeks or months) to test the solid-solid transition evolution. As  
262 expected, significant differences were observed. Baryshnikov demonstrated that while in the  
263 first run, II-NaNO<sub>3</sub> and b-KNO<sub>3</sub> coexist, in the second heating run, only the g-KNO<sub>3</sub> type  
264 solid solutions seem to be present,[28] consistent with the results of our DSC stability  
265 experiments. As a result, we have to point out that all the experimental information available  
266 conducts us to propose that the first heating run starts from a stable state. The numerical  
267 values of the heat effects at the eutectoid temperature, as beautifully follows from the data  
268 in Table 2, are linear in composition - in agreement with the lever rule.[68]

269 Furthermore, a transition, probably a  $\lambda$  transition or even a second order, is detected  
270 only for high sodium nitrate content. This transition and the melting signal overlapped one  
271 another for some compositions because the continuous variation of the slope, characteristic

272 from this transition, is supposed to be overlapped by the strong heat interchange of the  
273 melting signal.

274 In hot stage microscopy, only first-order solid-solid transitions could be studied, i.e.  
275 those related to KNO<sub>3</sub>. The a-b transition on heating and the b-g transition on cooling were  
276 not destructive. In contrast, the g-a transition is totally destructive causing crystals or  
277 domains to break into smaller pieces. Furthermore, since g-phase is metastable at room  
278 temperature, the transition time changes in different experiments and different compositions,  
279 as was described in the Introduction section. When the temperature is above the eutectoid  
280 temperature, all the crystal phase boundaries move fast and tend to grow to achieve the  
281 minimum free energy in accordance with the Tamman and Ruppelt work.[40]

### 282 *X-ray diffraction analyses at room temperature*

283 XRD analyses were carried out at room temperature to assess the crystal phases.  
284 Diffractograms were indexed as the combination a-KNO<sub>3</sub> and II-NaNO<sub>3</sub>, except for the  
285 extreme compositions (1% KNO<sub>3</sub> and 99% KNO<sub>3</sub>) in which only the pure components are  
286 observed.

287 For the extreme compositions, XRD revealed somewhat wider- and less defined peaks.  
288 Minor component peak intensities for these compositions, if any, may be very close to the  
289 detection limit of XRD so they cannot be resolved from background.

290 For compositions from 1% KNO<sub>3</sub> to 20% KNO<sub>3</sub>, a weak reflection at 27.10° of 2 $\theta$   
291 was visible, which can be assigned to the g-KNO<sub>3</sub> phase. According to Westphal,[23,24]  
292 the change g-KNO<sub>3</sub>  $\rightarrow$  a-KNO<sub>3</sub> can be considered as a cooperative phase transition. This  
293 explains that when the mass fraction is small, the transition is slower because each g-KNO<sub>3</sub>  
294 particle has to nucleate its own path for phase transition. Therefore, part of the g-KNO<sub>3</sub>  
295 phase can be retained as the result of a kinetic effect.

### 296 *Raman spectroscopy analyses at room temperature*

297 The narrow miscibility range at room temperature was confirmed by macro Raman  
298 measurements of 19 samples, including pure compounds. Figure 2 shows the most important  
299 band positions and intensities, corresponding to the N-O stretching mode n1 at 1068 cm<sup>-1</sup>  
300 and at 1049 cm<sup>-1</sup> for NaNO<sub>3</sub> and KNO<sub>3</sub>, respectively.[69] Intensity values are almost linear  
301 with composition, and the position of bands does not change within the experimental error.  
302 If sodium and potassium nitrate are miscible at room temperature, their miscibility range

303 should be lower than 1%, which is in agreement with the results of Hissink [41] who stated  
304 that miscibility at room temperature was about 0.5%.

### 305 *X-ray diffraction analysis as a function of temperature*

306 As mentioned above, although this binary system has been studied for a long time,  
307 very few researchers have characterized mixed samples by XRD.

308 In Figure 3, the results are shown of our XRD experiments on samples having the  
309 equimolar composition studied from 301 K to melting temperature. Here, we observe that  
310 from room temperature to 373 K, a-KNO<sub>3</sub> and II-NaNO<sub>3</sub> phases coexist. At 393 K, a phase  
311 change takes place, confirming the existence of a eutectoid invariant in accordance with the  
312 DSC data. Following this, between 393 and 473 K, peaks appear that can be assigned to a b-  
313 KNO<sub>3</sub> solid solution, but they are not well developed (some of them are marked with an  
314 arrow). Practically all the system is out of equilibrium above the eutectoid invariant when  
315 we analyse each composition at 10 K/min. As explained above, the different phase regions  
316 are assigned with XRD where annealing is performed to arrive at the equilibrium. The  
317 transition temperatures observed by DSC and evaluated by XRD coincide. Finally, and of  
318 vital importance, is to mention the appearance of a completely developed unique phase at  
319 483 K - a result that is consistent with the findings of Kamimoto. [35] In fact, II-NaNO<sub>3</sub>  
320 diffraction peaks disappeared at 473 K, but transition was not complete because few peaks  
321 persist. If we compare diffraction at 473 and 483 K, we observe that only some peaks  
322 (encircled in Figure 4) persist while others disappear.

323 To proceed further, annealing experiments were carried out for selected compositions,  
324 at different temperatures and annealing times in order to reach the equilibrium state.

325 Figure 4 shows the integral breadth for (101) X-ray reflection of the b-solid solution  
326 type and (104) for I-NaNO<sub>3</sub> solid solution type as a function of annealing time for 20 KNO<sub>3</sub>  
327 at 483 K. These results demonstrate the importance of annealing time in achieving the  
328 equilibrium. It can be seen that the integral width for both reflections decreases and then  
329 reaches an almost constant value after approximately 50 hours of annealing. The same  
330 findings were observed for the peaks intensity. The solvus line (transition from two phases  
331 to one phase domain) cannot be measured by DSC because the transition is too slow and  
332 possibly the interchanged heat is small. Only the XRD at different temperatures permit us to  
333 determine this transition.

334 Samples of different compositions were kept for 48 hours at the four selected  
335 temperatures above the eutectoid invariant: 403, 433, 453 and 483 K, and then studied by  
336 the X-ray powder diffraction. For each temperature, the diffraction patterns are shown in  
337 Figure 5.

338 Figure 5(a), for 403 K, shows that the state of equilibrium is not yet achieved after 48  
339 h. For the compositions 20% and 40% KNO<sub>3</sub>, a single b-KNO<sub>3</sub> pattern type is observed  
340 together with (some peaks of) the II-NaNO<sub>3</sub> pattern. The b-KNO<sub>3</sub> reflections were displaced  
341 to 2u higher values compared to pure KNO<sub>3</sub>, indicating a smaller cell size, as a result of the  
342 introduction of sodium cations in the structure. Thus, a new phase appeared (as stated above),  
343 which was named b-solid solution because it has the same space group as b-KNO<sub>3</sub>, R3m. In  
344 contrast, the II-NaNO<sub>3</sub> pattern hardly changed, meaning that a significant amount of  
345 potassium did not enter the R3c structure of NaNO<sub>3</sub>.

346 Figure 5(b), for 433 K, shows that for the 70% KNO<sub>3</sub> composition, only the b-solid  
347 solution is present, although it is not completely stable because the diffraction peaks are still  
348 relatively wide. For the remaining compositions analysed, the coexistence of b-solid solution  
349 and II-NaNO<sub>3</sub> patterns is observed, with a constant angle of 2u, typical of an immiscibility  
350 zone.

351 In Figure 5(c), for 453 K, we notice that for the equimolar composition, the II-NaNO<sub>3</sub>  
352 type reflections have almost disappeared; only a minor II-NaNO<sub>3</sub> (104) reflection remains.  
353 This indicates an increasing presence of the b-solid solution, incorporating more sodium in  
354 its structure. For the 20% KNO<sub>3</sub> diffraction pattern, reflections due to II-NaNO<sub>3</sub> were  
355 slightly displaced to lower 2u angle values (i.e. a larger unit cell) indicating that an amount  
356 of potassium is incorporated into its structure. Furthermore, a weak reflection at 21.6° is  
357 present, which can be indexed as (101) for the coexisting R3m phase (b-KNO<sub>3</sub> solid  
358 solution).

359 In Figure 5(d), for 483 K, the samples having compositions of 40% KNO<sub>3</sub> and higher  
360 are found to be homogeneous (b-solid solution space group R3m). For lower potassium  
361 concentrations, a mixture between the b-solid solution and the II-NaNO<sub>3</sub> solid solution is  
362 observed. The diffraction lines of the R3c (II-NaNO<sub>3</sub>) phase are displaced to lower 2u angles  
363 compared to pure NaNO<sub>3</sub>, indicating a higher unit cell compatible with the introduction of  
364 potassium in its structure, as explained above. Although the II-NaNO<sub>3</sub> solid solution single-

365 phase domain must exist, we were unable to isolate it even by performing similar ageing  
366 experiments for the 5% KNO<sub>3</sub> composition.

367 From the previous analysis, we can deduce the space group and cell parameters, using  
368 the Materials Studio software.[64] Figure 6 shows the cell parameters (a and c) for these  
369 compositions together with pure KNO<sub>3</sub> and pure NaNO<sub>3</sub>. As shown, Vegard's law is obeyed  
370 until 40% KNO<sub>3</sub>, i.e. in all single-phase regions. For 40% KNO<sub>3</sub>, 50% KNO<sub>3</sub>, 70% KNO<sub>3</sub>  
371 and 90% KNO<sub>3</sub>, a solution with the R3m symmetry was obtained. In all cases, the agreement  
372 between the experimental and simulated pattern expressed by the weighted R-factor (R<sub>wp</sub>)  
373 was below 7%.

374 If we extrapolate the lines, we observe that they cut at approximately a and c/2  
375 parameter for NaNO<sub>3</sub> composition; c parameter in NaNO<sub>3</sub> is halved in order to compare the  
376 same space group in both structures.[7]

377 When annealing is performed at 493 K, for 20% KNO<sub>3</sub> composition, the peaks of the  
378 II-NaNO<sub>3</sub> solid solution tend to disappear (results not shown). Nevertheless, 48 h was not  
379 enough time for completing the transition. We conclude that a single phase is also present in  
380 this composition but at higher temperatures.

381 All these results lead us to the main result of the paper: the experimental phase diagram  
382 shown in Figure 7. We assume that below the eutectoid, the solubility of Na + in a-KNO<sub>3</sub> is  
383 slightly higher than K + in the II-NaNO<sub>3</sub> structure, when kept at the same temperature. This  
384 is consistent with the fact that it is easier to introduce a smaller cation into a structure of  
385 larger cations than in the opposite case. Both the b-KNO<sub>3</sub> solid solution type and the II-  
386 NaNO<sub>3</sub> solid solution type have a narrow domain of existence with a maximum solubility  
387 at 393 (eutectoid invariant) and 483 K, respectively. Above the eutectoid invariant, we  
388 observed a very asymmetric immiscibility gap and a large domain of b-KNO<sub>3</sub> solid solution  
389 type, which is present throughout compositions for certain temperature ranges. The second-  
390 order transition (or  $\lambda$  transition) can end wherever but we chose at the top of this  
391 immiscibility gap for the sake of simplicity. Finally, solid-liquid biphasic equilibrium with  
392 a flat minimum at 495 K was inferred.

393

394

395

396 ***Thermodynamic assessment***

397 The aim of our thermodynamic analysis is two-fold. On the one hand, it aims to explore  
 398 to which extent the underlying system complies with the general characteristics found for  
 399 mixed crystals. On the other hand, it aims to assess to which extent the phase diagram, Figure  
 400 7, is consistent with the thermochemical data that are available for the system itself

401 To start with, and as regards the characteristics of mixed crystals, recent research has  
 402 shown that their thermodynamic mixing properties are well accounted by the ABu model for  
 403 the excess Gibbs energy, see Oonk and references therein.[30]

404 In terms of the ABu model, the molar excess Gibbs energy, as a function of  
 405 temperature and mole fraction of the second component (here KNO<sub>3</sub>) is given by the  
 406 following expression:

$$407 \quad G^E(T, X) = AX(1 - X) \left(1 - \frac{T}{\theta}\right) [1 + B(1 - 2X)] \quad (1)$$

408 where A, B and u are system-dependent parameters. The parameter A (in J·mol<sup>-1</sup>) represents  
 409 the magnitude of the excess function; u (in K) the function's dependence on temperature;  
 410 and B (dimensionless) the asymmetry of the function. The form in X between the square  
 411 brackets has the advantage that the excess function of the equimolar mixture does not contain  
 412 the parameter B.

413 The fact that GE is linear in temperature implies that the excess enthalpy does not  
 414 change with temperature:

$$415 \quad H^E(T, X) \rightarrow H^E(X) = AX(1 - X) [1 + B(1 - 2X)] \quad (2)$$

416 Another characteristic of the ABu model is the fact that the mole fraction of the critical  
 417 point of mixing ( $X_c$ ) is the solution of the quadratic equation:

$$418 \quad (18B)X^2 - (2 + 18B)X + (1 + 3B) = 0 \quad (3)$$

419 Next, the critical temperature of mixing ( $T_c$ ) is obtained on the substitution of  $X_c$ 's  
 420 value in

$$421 \quad T(X_c) = \frac{[2A + 6AB(1 - 2X_c)X_c(1 - X_c)]}{R + (1/\theta)[2A + 6AB(1 - 2X_c)X_c(1 - X_c)]} \quad (4)$$

422 An intriguing aspect of mixed crystals is the existence of an empirical relationship  
423 between the value of the model parameter  $u$  and the melting temperature ( $T_m$ ) of the  
424 equimolar mixture:

$$425 \quad \frac{\log (\theta / K)}{\log \left(T_m / K\right)} = 1.10 \pm 0.05 \quad (5)$$

426 At this place, we may observe that the melting point of the equimolar mixture together  
427 with the coordinates of the critical point of mixing are capable of giving a first impression  
428 of the values of the system-dependent parameters  $A$ ,  $B$  and  $u$ .

429 For the system at hand, we have  $T_m$  D 494 K;  $T_c$  D 448 K and  $X_c$  between 0.4 and  
430 0.5. The last of these values goes well with  $B$  D 0.1, for which  $X_c$  D 0.43. An opening to the  
431 value of  $u$  is offered by Equation (5):  $u$  D 920 K; for  $T_m$  D 494 K. The value of parameter  
432  $A$  follows from Equation (4) with  $T_c$  D 448 K;  $B$  D 0.1;  $u$  D 920 K;  $X_c$  D 0.43; and the value  
433 of  $8.314472 \text{ J}\cdot\text{mol}^{-1}\cdot\text{K}^{-1}$  for the gas constant  $R$ ; the result is  $A$  D  $14250 \text{ J}\cdot\text{mol}^{-1}$ .

434 In the remaining part of our analysis, we concentrate on the change from solid to liquid  
435 of the equimolar mixture in terms of thermochemistry. The key thermochemical quantities  
436 are the change in enthalpy and the change in the Gibbs energy. The limited influence of the  
437 difference between the heat capacities of the liquid and solid states will be ignored. The  
438 change in enthalpy is an opening to the difference between the excess enthalpies of liquid  
439 and solid. Likewise, the change in the Gibbs energy is an opening to the difference between  
440 the excess Gibbs energies of liquid and solid. The numerical values that are needed for our  
441 calculations are taken from Rogers and Janz.[36] Their data are essentially the same as ours,  
442 see Table 2, though somewhat more precise.

443 For the equimolar mixture, the change in enthalpy from solid to liquid is given by the  
444 expression

$$445 \quad \Delta H (X = 0.5) = 0.5\Delta H_A^* + 0.5\Delta H_B^* + \Delta H^E (X = 0.5), \quad (6)$$

446 in which  $\Delta H_A^*$  and  $\Delta H_B^*$  stand for the enthalpies of melting of pure  $A = \text{NaNO}_3$  and  
447 pure  $B = \text{KNO}_3$ ; an asterisk as a superscript is used to refer to a pure-component quantity.  
448 After substitution of the experimental data, Equation (6) changes into

$$449 \quad 9370 = 0.5 \times 15440 + 0.5 \times 10020 + \Delta H^E (X = 0.5)/\text{J}\cdot\text{mol}^{-1} \quad (7)$$

450



451 From Equation (7), the equimolar change in excess enthalpy is calculated as

$$452 \quad \Delta H^E (X = 0.5) = -3360 \text{ J} \cdot \text{mol}^{-1} \quad (8)$$

453 Unlike the difference in enthalpy, the difference in the Gibbs energy is not independent  
454 of temperature:

$$455 \quad \Delta G (T, X = 0.5) = 0.5\Delta G_A^* (T) + 0.5\Delta G_B^* (T) + \Delta G^E (X = 0.5), \quad (9)$$

456 The quantities  $\Delta G_A^* (T)$  and  $\Delta H_B^* (T)$  which represent the change in the Gibbs energy  
457 on melting, are composed of an enthalpy and an entropy part as

$$458 \quad \Delta G_A^* (T) = \Delta H_A^* - T \Delta S_A^* \text{ and similar for component B} \quad (10)$$

459 in which  $\Delta S_A^*$ , the entropy of melting, is the quotient of A's enthalpy of melting and its  
460 melting point.

461 Inserting all numerical values in Equations (9) and (10) for T D 494 K, one obtains

$$462 \quad \Delta G (T = 494\text{K}, X = 0.5) = 0 = 0.5 (15440 - 26.67 \times 494) + 0.5 (10020 - 16.48 \times 494) \\ 463 \quad + \Delta G^E (T = 494\text{K}, X = 0.5) \quad (11)$$

464 In the first line of Equation (11), the zero between the two signs of equality is to  
465 indicate that the difference in the Gibbs energy is zero. This is the consequence of the fact  
466 that the two phases in equilibrium have the same composition, which is X D 0.5. From  
467 Equation (11),

$$468 \quad \Delta G^E (X = 0.5) = -2072 \text{ J} \cdot \text{mol}^{-1} \quad (12)$$

469 The last step of the evaluation of the equimolar excess properties of the mixed  
470 crystalline solid state is shown in Table 3.

471 In Table 3, the data for the liquid state are based on experimental heat of mixing data  
472 published by Kleppa.[70] These data were subjected to the empirical relationships found for  
473 binary liquid mixtures of common-ion alkali halides, to yield the excess values of -525 and  
474 -350 J·mol<sup>-1</sup>.[71,72]

475 Through Equations (1) and (2), the solid state data in Table 3 give rise to A = 11340  
476 J·mol<sup>-1</sup> and u = 1258 K. Along with B = 0.1, the computed A and u yield 448 K for the  
477 critical temperature of solid mixing, which is precisely the experimental temperature.

478 The fact that the computed result,  $T_c = 448$  K, coincides with the experimental value  
479 for the critical temperature is satisfactory. A fact is, of course, that the outcome of the  
480 computations is sensitive to changes in the input data. The outcome is especially sensitive to  
481 the numerical value of the (difference) excess Gibbs energy. To give an example: when the  
482 excess Gibbs energy of the liquid is changed from  $\bar{g}350$  to  $\bar{g}250$  J·mol<sup>-1</sup>, all other things  
483 being equal, the value of  $u$  changes from 1258 to 1383 K, and subsequently the critical  
484 temperature from 448 to 463 K.

485 The outcome of the thermodynamic analysis is summarized in Table 4.

486 The numerical values in the bottom row of Table 4 for the three parameters model of  
487 the solid state, along with the melting properties of the pure components and the excess  
488 properties of the liquid state, were used to calculate the phase diagram. More precisely, the  
489 diagram the system would have if there were no phase transition in solid sodium nitrate. The  
490 calculated diagram is shown in Figure 8. The opening angle of the two-phase region in the  
491 lower right-hand corner of the diagram was calculated using Van't Hoff's law (see Oonk  
492 and Calvet).[68]

493 An inspection of Figures 7 and 8 reveals that the two diagrams look very much alike.  
494 Clearly, the AB $\theta$  model is fully capable of giving a thermodynamically sound description of  
495 the sub-solidus solid state. In this respect, the NaNO<sub>3</sub> + KNO<sub>3</sub> system's behaviour is fully  
496 in line with the behaviour elucidated for the alkali halide systems, and mixed-crystal systems  
497 in general.

498 Our calculated and experimental results agree very well in the sense that the calculated  
499 diagram reproduces the asymmetric miscibility gap and the high-temperature single-phase  
500 domain.

501

502

503

504

## 505 2. DISCUSSION

506 The NaNO<sub>3</sub>-KNO<sub>3</sub> phase diagram has been studied for more than 150 years. As  
507 outlined in this paper, it is easy to understand the difficulties in developing an accurate  
508 unique phase diagram. While some studies demonstrated the presence of solid-liquid  
509 equilibrium with a minimum, others justify a eutectic invariant. It is, in fact, not surprising  
510 because the system is complex and certain experimental precautions must be considered.  
511 Transition kinetics, metastability and second-order transition are difficulties that arise from  
512 the experimental study. The diagram presented here is a representation of equilibrium state.

513 Figure 1 shows, as much as possible, the polymorphic behaviour of NaNO<sub>3</sub> and  
514 KNO<sub>3</sub>. It is important to consider that a necessary but not sufficient condition to achieve  
515 total miscibility in solid state is that components crystallize in the same spatial group. At  
516 room temperature, phase II NaNO<sub>3</sub> crystallizes in the R3c spatial group and the a-KNO<sub>3</sub>  
517 phase crystallizes in the Pnma group. Total miscibility at room temperature is impossible.  
518 Our experimental and theoretical results show that the miscibility at the room temperature  
519 in this binary system is reduced. However, the situation is more complicated because if  
520 KNO<sub>3</sub> is melted, then the g-KNO<sub>3</sub> phase is formed during the cooling and coexistence of  
521 II-NaNO<sub>3</sub> and g-KNO<sub>3</sub> becomes possible. Nevertheless, in this case, total miscibility is also  
522 impossible (g-KNO<sub>3</sub> crystallizes in the R3m group). In conclusion, an immiscibility gap is  
523 theoretically expected and experimentally confirmed at room temperature for this binary  
524 system.

525 At higher temperatures (401 K), Pnma a-KNO<sub>3</sub> transforms into an R3m b-KNO<sub>3</sub> by a  
526 first-order transition. Following the phase rule, a two phase domain with a-KNO<sub>3</sub> and b-  
527 KNO<sub>3</sub> is required. Effectively, our experimental and theoretical results show us this two  
528 solid phase domain. The first-order transition conduces to a eutectoid invariant at 393 K, and  
529 to a high-temperature miscibility domain, thus the solid-liquid equilibrium is present.  
530 Equilibrium between two solid solutions, one rich in II-NaNO<sub>3</sub> and the other rich in b-  
531 KNO<sub>3</sub>, exists.

532 For sodium nitrate, a second-order transition from the II-NaNO<sub>3</sub> phase to the I-NaNO<sub>3</sub>  
533 phase is present. The R3m I-NaNO<sub>3</sub> phase is isostructural with the high temperature R3m  
534 b-KNO<sub>3</sub>. Second-order transitions are not always considered in the literature for the phase  
535 diagram determination; however, in this case, it is crucial for the isomorphic relationships

536 analysis between NaNO<sub>3</sub> and KNO<sub>3</sub>. For this transition type, only the final temperature can  
537 be determined by a DSC analysis.

538 The question that has remained unanswered for over 150 years is: Does the solvus  
539 intersect with the solidus? To solve this question, experimental precautions regarding  
540 metastability must be taken into account. To achieve equilibrium at a high temperature, a  
541 minimum of 48 hours is required (depending on the composition and the temperature).  
542 Without this annealing period, a metastable mixture of different phases is observed. A solid  
543 solution (named in this study as b-KNO<sub>3</sub> solid solution) between isostructural R3m I-  
544 NaNO<sub>3</sub> and R3m b-KNO<sub>3</sub> exists. In some compositions, it is only present within a narrow  
545 temperature range just below the solidus line. At this stage, we can confirm that INaNO<sub>3</sub>  
546 and b-KNO<sub>3</sub> are isomorphous, that the binary system between NaNO<sub>3</sub> and KNO<sub>3</sub> is a  
547 system with high-temperature total miscibility, and that the solid-liquid equilibrium is a two-  
548 phase domain with a minimum.

549 At the atomic level, R3m I-NaNO<sub>3</sub> and R3m b-KNO<sub>3</sub> are essentially the same. Static  
550 and dynamic disorder has been proposed for b-KNO<sub>3</sub>, see Nimmo and Lucas [20] and  
551 references therein for more information. They proposed that the NO<sub>3</sub><sup>-</sup> group is not planar  
552 (in KNO<sub>3</sub>) and thus a structural difference between I-NaNO<sub>3</sub> and b-KNO<sub>3</sub> is possible  
553 (although they have the same space group). In contrast, Stromme [31,73] made least squares  
554 refinement of both R3m structures, I-NaNO<sub>3</sub> (at 563 K) and b-KNO<sub>3</sub> (at 425 K) and arrived  
555 at the same solution: disorder at high temperature can be modelled in the same manner.  
556 Slight differences in the structures are accepted and thus, interchanging between Na<sup>+</sup> and  
557 K<sup>+</sup> is possible particularly at high temperatures. Therefore, we can say that R3m I-NaNO<sub>3</sub>  
558 and R3m b-KNO<sub>3</sub> are isomorphous at high temperature.

559

560

561

562

563

### 564 3. CONCLUSIONS

565 The main result of this work is the experimental phase diagram proposed. It has a  
566 eutectoid invariant at 393 K, with an extended immiscibility zone below this invariant, with  
567 very limited solid solutions at both extremes. Above the eutectoid invariant, there is an  
568 asymmetric immiscibility gap, and the NaNO<sub>3</sub> second order transition can end in the  
569 uppermost point of the immiscibility gap. A narrow NaNO<sub>3</sub> R3c solid solution domain must  
570 exist below; however, this was not observed directly. Furthermore, at high temperatures, a  
571 b-KNO<sub>3</sub> solid solution is observed for all compositions, thus, the phase diagram shows a  
572 solid-liquid equilibrium with minimum. Therefore, I-NaNO<sub>3</sub> and b-KNO<sub>3</sub> are only  
573 isomorphous at high temperatures because they are isostructural, chemically analogous and  
574 can form a solid solution in all compositions.

575 Our study has revealed that slow transition kinetics for the formation of high-  
576 temperature solid solutions can explain the conflicting arguments that exist in the literature  
577 to solve whether the diagram is eutectic or melting point minimum.

578 Thermodynamic results of the analysis are not in conflict with the experimental  
579 evidence for (complete) subsolidus miscibility. Finally, the phase diagram of the system  
580 NaNO<sub>3</sub> - KNO<sub>3</sub> and its thermodynamic mixing properties are fully in line with the general  
581 characteristics found for the mixed crystal systems.

582

583

584

585

586

587

588

589

590 **DISCLOSURE STATEMENT**

591 No potential conflict of interest was reported by the authors.

592

593

594

595

596

597

598

599

600 **FUNDING**

601 This work was supported by the Ministerio de Ciencia y Tecnología [grant CICYT  
602 (MAT2011-27225)]; the Generalitat de Catalunya under grant Grup Consolidat  
603 [2009SGR1307], and Xarxa de Referència RCDCI en Materials Avançats per l'Energia  
604 (XaRMAE). And The Ministerio de Educación on under grant la Factoría Cristalográfica  
605 [Consolider-Ingenio CSD2006-15]. R. Benages-Vilau acknowledges Abengoa enterprise for  
606 the financial support through a Cenix program Consorcio Solar de I+D ConSOLi+da.

607

608

609

610

611

612

613

614 **REFERENCES**

- 615 [1] Berg RW, Kerridge DH. The NaNO<sub>3</sub>-KNO<sub>3</sub> system: the position of the solidus and  
616 sub-solidus. Dalton Trans. 2004;15:2224-2229.
- 617 [2] Voskresenskaya NK, Evseeva NN, Berul SI. Handbook of solid-liquid equilibria in  
618 systems of anhydrous inorganic salts. Jerusalem: Keter Press; 1970. Part I, Binary  
619 systems with common anion; p. 7-602.
- 620 [3] Berg RW, Kerridge DH. Raman mapping in the elucidation of solid salt eutectic and  
621 near eutectic structures. J Raman Spec. 2002;33:165-172.
- 622 [4] Benes O, Konings R, Wurzer S, et al. A DSC study of the NaNO<sub>3</sub>-KNO<sub>3</sub> system using  
623 an innovative encapsulation technique. Thermochim Acta. 2010;509:62-66.
- 624 [5] Ping W, Harrowell PBN, Angell CA. Composition dependence of the solid state  
625 transitions in NaNO<sub>3</sub>/KNO<sub>3</sub> mixtures. Thermochim Acta. 2009;486:27-31.
- 626 [6] Rao CNR, Prakash B, Natarajan M. Crystal structure transformations in inorganic  
627 nitrites, nitrates, and carbonates. National Standard Reference Data System - National  
628 Bureau of Standards; 1975.
- 629 [7] Benages-Vilau R, Calvet T, Cuevas-Diarte MA. Polymorphism, crystal growth, crystal  
630 morphology and solid state miscibility of alkali nitrates. Crystall Rev. 2014;20(1):25-  
631 55.
- 632 [8] Paul GL, Pryor AW. Study of sodium-nitrate by neutron diffraction. Acta Cryst B.  
633 1972;28:2700-2702.
- 634 [9] Gonschorek G, Weitzel H, Miede G, et al. The crystal structure of NaNO<sub>3</sub> at 100 K,  
635 120 K, and 563K. Zeitschrift für Kristallographie. 2000;215:752-756.
- 636 [10] Fermor JH, Kjekshus A. On the electrical properties of NaNO<sub>3</sub>. Acta Chem Scand.  
637 1968;22:1628-1636.
- 638 [11] Parsonage NG, Staveley LAK. Disorder in crystals. Oxford: Clarendon Press; 1978.
- 639 [12] Klement WJ. Variation of  $\lambda$  transition temperature in NaNO<sub>3</sub>-base binary alloys with  
640 AgNO<sub>3</sub>, KNO<sub>3</sub>, and NaNO<sub>2</sub>. J Inorg Nucl Chem. 1974;36:1916-1918.
- 641 [13] Antao SM, Hassan I, Mulder WH, et al. The R-3c  $\rightarrow$  R-3 m transition in nitratine,

- 642 NaNO<sub>3</sub>, and implications for calcite, CaCO<sub>3</sub>. *Phys Chem Minerals*. 2008;35:545-557.
- 643 [14] Antao SM, Hassan I, Mulder WH, et al. In situ of the R-3c !R-3 m orientational  
644 disorder in calcite. *Phys Chem Minerals*. 2009;36:159-169.
- 645 [15] Ballirano P. Laboratory parallel-beam transmission X-ray powder diffraction  
646 investigation of the thermal behavior of nitratine NaNO<sub>3</sub>: spontaneous strain and  
647 structure evolution. *Phys Chem Minerals*. 2011;38:531-541.
- 648 [16] Harris MJ. A new explanation for the unusual critical behaviour of calcite and sodium  
649 nitrate, NaNO<sub>3</sub>. *Am Mineralogist*. 1999;84:1632-1640.
- 650 [17] Zamali H, Jemal M. Diagrammes de phases des systemes binaires KNO<sub>3</sub>-CsNO<sub>3</sub> et  
651 KNO<sub>3</sub>-NaNO<sub>3</sub>. *J Thermal Anal*. 1994;41:1091-1099.
- 652 [18] Dessureault Y, Sangster J, Pelton AD. Evaluation critique des données  
653 thermodynamiques et des diagrammes de phases des systèemes AOH-AX, ANO<sub>3</sub>-AX,  
654 ANO<sub>3</sub>-BNO<sub>3</sub>, AOX, BOX où A, B = Li, Na, K Et X = Cl, F, NO<sub>3</sub>, OH. *J Chim Phys*.  
655 1990;87:407-453.
- 656 [19] Chen A, Chernow F. Nature of ferroelectricity in KNO<sub>3</sub>. *Phys Rev*. 1967;154:493-  
657 505.
- 658 [20] Nimmo JK, Lucas BW. The crystal structures of g- and b-KNO<sub>3</sub> and the a, b,g phase  
659 transformations. *Acta Cryst*. 1976;B-32:1968-1971.
- 660 [21] Shimada S, Aoki T. Stabilization of the ferroelectric g-phase by doping with Na<sup>+</sup>  
661 determined by the acoustic emission method. *Chem Lett*. 1996;393-394
- 662 [22] Christensen AN, Norby P, Hanson JC, et al. Phase transition of KNO<sub>3</sub> monitored by  
663 sincrotrón X-ray powder diffraction. *Appl Cryst*. 1996;29:265-269.
- 664 [23] Westphal MJ. Particle size and cooperative behaviour effects on KNO<sub>3</sub> phase  
665 transitions. *J Appl Phys*. 1993;74:6107-6114.
- 666 [24] Westphal MJ. Cooperative behavior during ferroelectric transition in KNO<sub>3</sub> powder.  
667 *J Appl Phys*. 1993;74:3131-3136.
- 668 [25] Westphal MJ, Wood JW, Redin RD, et al. Calorimetric and photoacoustic investigation  
669 of KNO<sub>3</sub> phase transition. *J Appl Phys*. 1993;73:7302-7310.
- 670 [26] Shimada S, Katsuda Y, Inagaki M. Phase transition of potassium nitrate monitored by



- 671 acoustic emission technique and the healing effect on the g-a transition. *J Phys Chem.*  
672 1993;97:8803-8807.
- 673 [27] Poprawski R, Rysiakiewicz-Pasek E, Sieradzki A, et al. Ferroelectric phase transitions  
674 in KNO<sub>3</sub> embedded into porous glasses. *J Non Cryst Solids.* 2007;353:4457-4461.
- 675 [28] Baryshnikov SV, Charnaya EV, Milinkiy AY, et al. Phase transition in K<sub>1-x</sub>Na<sub>x</sub>NO<sub>3</sub>  
676 embedded into molecular sieves. *J Phys Cond Mat.* 2009;21:325902.
- 677 [29] Fermor JH, Kjekshus A. On the electrical properties of KNO<sub>3</sub>. *Acta Chemica*  
678 *Scandinavica.* 1967;21:1265-1276.
- 679 [30] Oonk HAJ. Solid-state solubility and its limits. The alkali halide case. *Pure Appl*  
680 *Chem.* 2001;73:807-823.
- 681 [31] Stromme KO. On the crystal structure of potassium nitrate in the high temperature  
682 phases I and III. *Acta Chemica Scandinavica.* 1969;23:1625-1636.
- 683 [32] Xu K, Chen Y. Raman spectroscopic studies of mixed crystals of NaNO<sub>3</sub>-KNO<sub>3</sub>  
684 quenched from different temperatures: evidence for limited solid solutions in the  
685 system. *J Raman Spectrosc.* 1999;30:441-448.
- 686 [33] Greis O, Bahamadan KM, Uwais BM. The phase diagram of the system NaNO<sub>3</sub>-  
687 KNO<sub>3</sub> studied by differential scanning calorimetry. *Thermochim Acta.* 1985;86:343-  
688 350.
- 689 [34] Kramer CM, Wilson CJ. The phase diagram of NaNO<sub>3</sub>-KNO<sub>3</sub>. *Thermochim Acta.*  
690 1980;42:253-264.
- 691 [35] Kamimoto M. Thermodynamic properties of 50 Mole% NaNO<sub>3</sub>-50KNO<sub>3</sub> [HTS2].  
692 *Thermochim Acta.* 1981;49:319-331.
- 693 [36] Rogers DJ, Janz GJ. Melting-crystallization and premelting properties NaNO<sub>3</sub>-  
694 NaNO<sub>3</sub> enthalpies and heat capacities. *J Chem Eng Data* 1982;27:424-428.
- 695 [37] Abe O, Utsunomiya T, Hoshino Y. The thermal stability of binary alkali metal nitrates.  
696 *Thermochim Acta.* 1984;78:251-260.
- 697 [38] Zamali H, Jriri R, Rogez J, et al. Mixing properties in the continuous solid solution of  
698 the system KNO<sub>3</sub>-NaNO<sub>3</sub>. *Thermochim Acta.* 1994;233:111.
- 699 [39] Zhang X, Tian J, Xu K, et al. Thermodynamic evaluation of phase equilibria in

- 700 NaNO<sub>3</sub>-KNO<sub>3</sub> systems. *J Phase Equilibria*. 2003;24:441-446.
- 701 [40] Tammann VG, Ruppelt A. Die entmischung lückenlose mischkristallreihen [The  
702 segregation gaps of solid solution series]. *Zeitschrift für anorganische und allgemeine*  
703 *Chemie*. 1931;197:65-89.
- 704 [41] Hissink DJ. On the formation and conversion of mixed crystals from sodium nitrate  
705 and potassium nitrate and from sodium nitrate with silver nitrate. *Z Phys Chem*.  
706 1900;32:537-563.
- 707 [42] Madgin WM, Briscoe HVA. The melting point [solidus] curve for mixtures of  
708 potassium nitrate and sodium nitrate. *J Chem Soc*. 1923;123:2914-2916.
- 709 [43] Briscoe HVA, Madgin W M. The freezing point curve for mixtures of potassium  
710 nitrate and sodium nitrate. *J Chem Soc*. 1923;123:1608-1618.
- 711 [44] Kofler VA. Über Periodische Umlagerungen Beim Kristallisieren Und Schmelzen  
712 Von Mischkristallen *Z Elektrochem*. [Rearrangements crystallization and melting of  
713 mixed crystals]. 1955;59:939-941.
- 714 [45] Bartlett HE, Johnson KE. Electrolytic reduction and ellingham diagrams for oxy-  
715 anions systems. *Can J Chem*. 1966;44:2119-2129.
- 716 [46] Freeman ES. The kinetics of the thermal decomposition of sodium nitrate and of the  
717 reaction between sodium nitrite and oxygen. *J Phys Chem*. 1956;60:1487-1493.
- 718 [47] Freeman ES. The kinetics of the thermal decomposition of potassium nitrate and of  
719 the reaction between potassium nitrite and oxygen. *J Am Chem Soc*. 1957;79:838-842.
- 720 [48] Alexander JJ, Hindin SG. Phase relations in heat transfer salt systems. *Ind Eng Chem*.  
721 1947;39:1044-1049.
- 722 [49] Bartholomew RF. A study of the equilibrium  $\text{KNO}_3[\text{l}] \leftrightarrow \text{KNO}_2[\text{l}] + 1/2\text{O}_2[\text{g}]$  over  
723 the temperature range 550-750 °C. *J Phys Chem*. 1966;70:3442-3446.
- 724 [50] Carling RW. Heat capacities of NaNO<sub>3</sub> and KNO<sub>3</sub> from 350 to 800 K. *Thermochim*  
725 *Acta* 1983;60:265-275.
- 726 [51] Iwadate Y, Okada I, Kawamura K. Density and heat capacity of molten NaNO<sub>2</sub>-KNO<sub>3</sub>  
727 mixtures. *J Chem Eng Data*. 1982;27:288-290.
- 728 [52] Robelin C, Chartrand P, Pelton AD. Thermodynamic evaluation and optimization of

729 the (NaNO<sub>3</sub> + KNO<sub>3</sub> + Na<sub>2</sub>SO<sub>4</sub> + K<sub>2</sub>SO<sub>4</sub>) System. *J Chem Thermodyn.* 2015;83:12-  
730 26.

731 [53] Xu K, Chen Y. Temperature-dependent raman spectra of mixed crystals of NaNO<sub>3</sub>-  
732 KNO<sub>3</sub>: evidence for limited solid solution. *J Raman Spectrosc.* 1999;30:173-179.

733 [54] Laybourn K, Madgin WM. On the measurement of mechanical properties of binary  
734 inorganic salt mixtures. *J Chem Soc.* 1932;28:857-866.

735 [55] Eweka EI, Kerridge DH. Non-ideal change of electrical conductivity on solidification  
736 and remelting of salt eutectics: 1. Oxyanion-based systems. *Solid State Ionics.*  
737 2006;177: 1245-1250.

738 [56] Eweka IE, Kerridge DH. Changes in electrical conductivity of salt eutectic through the  
739 melting point. *Phys Let A.* 1993;174:441-442.

740 [57] Moreno E, Cordobilla R, Calvet T, et al. Polymorphism of even saturated carboxylic  
741 acid from n-decanoic to n-eicosanoic acid. *New J Chem.* 2007;31:947957.

742 [58] Gbbode G, Negrier P, Mondieig D, et al. Polymorphism and solid-state miscibility in  
743 the pentadecanoic acid-heptadecanoic acid binary system. *Chem Phys Lipids*  
744 2008;154:6877.

745 [59] Metivaud V, Lefevre A, Ventolà L, et al. Hexadecane [C<sub>16</sub>H<sub>34</sub>] 1-hexadecanol  
746 [C<sub>16</sub>H<sub>33</sub>OH] binary system: crystal structures of the components and experimental  
747 phase diagram. Application to thermal protection of liquids. *Chem Mat.*  
748 2005;17:33023310.

749 [60] Ventolà L, Calvet T, Cuevas-Diarte MA, et al. Solid-solid and solid-liquid equilibria  
750 in the nalkanols family: C<sub>18</sub>H<sub>37</sub>OH-C<sub>20</sub>H<sub>41</sub>OH system. *Phys Chem Chem Phys.*  
751 2004;6:37263731.

752 [61] Ventolà L, Metivaud V, Bayes L, et al. The binary system tetradecanedioic acid-  
753 hexadecanedioic acid: polymorphism of the components and experimental phase  
754 diagram. *Helvetica Chim Acta.* 2006;89:20272039.

755 [62] Ventolà L, Bayes L, Benages R, et al. Decanedioic acid [C<sub>10</sub>H<sub>18</sub>O<sub>4</sub>]/dodecanedioic  
756 acid [C<sub>12</sub>H<sub>22</sub>O<sub>4</sub>] system: polymorphism of the components and experimental phase  
757 diagram. *Helvetica Chim Acta.* 2008;91:12861298.

- 758 [63] Quality chemicals [Internet]. Spain. Available from:  
759 <http://www.qualitychemicals.com/cas/index.html>
- 760 [64] Courchinoux R, Chanh NB, Haget Y, et al. Du Signal aux Phenomenes: Une Approche  
761 Pratique l'Etablissement des Diagrammes de Phases par Analyse Thermique [Signal  
762 to phenomena: a practical approach to establishment of the phase diagrams of by  
763 thermal analysis]. *J Chim Phys.* 1989;86:561593.
- 764 [65] Materials studio modeling 4.2. [Internet]. Available from:  
765 <http://accelrys.com/products/materials-studio>
- 766 [66] Neumann M. X-Cell: a novel indexing algorithm for routine tasks and difficult cases.  
767 *J Appl Cryst.* 2003;36:356365.
- 768 [66] Pawley GS. Unit-cell refinement from powder diffraction scans. *J Appl Cryst.*  
769 1981;14:357361.
- 770 [68] Oonk HAJ, Calvet T. Equilibrium between phases of matter: phenomenology and  
771 thermodynamics. Dordrecht: Springer; 2008.
- 772 [69] Nakamoto K. Inorganic compounds; infrared and raman spectra of inorganic and  
773 coordination compounds. New York (NY): Wiley; 1986.
- 774 [70] Kleppa OJ. A new twin high-temperature reaction calorimeter. The heats of mixing in  
775 liquid sodium-potassium nitrates. *J Phys Chem.* 1960;64:19371940.
- 776 [71] Oonk HAJ, Bouwstra JA, van Ekeren PJ. Binary common-anion alkali halides  
777 mixtures, correlation of the thermochemical and phase diagram data. *Calphad.*  
778 1986;10:137161.
- 779 [72] van der Kemp WJM, Blok JG, van Genderen ACG, et al. Binary common-ion alkali  
780 halide mixtures: a uniform description of the liquid and solid state. *Thermochim Acta.*  
781 1992;196:301315.
- 782 [73] Stromme KO. The crystal structure of sodium nitrate in the high temperature phase.  
783 *Acta Chemica Scandinavica.* 1969;23:16161624.
- 784
- 785

786 **Table 1.** Selected cell parameters for NaNO<sub>3</sub> and KNO<sub>3</sub> phases.

787

Phase	$a/\text{Å}$	$b/\text{Å}$	$c/\text{Å}$	Ref.
I – NaNO <sub>3</sub> –R $\bar{3}c$	5.070		16.82	[8]
II – NaNO <sub>3</sub> –R $\bar{3}m$	5.0889(5)		8.868(3)	[9]
$\alpha$ -KNO <sub>3</sub> Pnma	6.4213	5.4119	9.1567	[7]*
$\beta$ -KNO <sub>3</sub> R $\bar{3}m$	5.425(1)		9.836(4)	[19]
$\gamma$ -KNO <sub>3</sub> R3m	5.487(1)		9.156(3)	[19]

788 Note: \*after transforming the Pmcn space group to the international accepted by IUCr.

789

790

791

792

793

794

795

796

797

798 **Table 2.** Results for temperatures and enthalpies of phase transitions for the NaNO<sub>3</sub>-KNO<sub>3</sub>  
 799 system.

800

(% mol KNO <sub>3</sub> )	Solid–solid transition					Solid–liquid transition			
	$T_{\alpha \rightarrow \beta}$ (K)	$T_{\text{end (II} \rightarrow \text{I)}}$ (K)	$T_{\text{eutectoid}}$ (K)	$T_{\text{(end eutectoid)}}$ (K)	$\Delta H_{s-s}$ (J.mol <sup>-1</sup> )	$T_{\text{melting}}$ (K)	$T_{\text{solidus}}$ (K)	$T_{\text{liquidus}}$ (K)	$\Delta H_{s-l}$ (J.mol <sup>-1</sup> )
0		544				581			15,435
10			394	398	410		494	567	13,433
20			395	397	930		494	545	12,561
30			394	395	1699		495	535	10,926
40			392	402	2180		494	503	10,223
50			396	399	2616		492	492	10,009
60			390	398	3192		495	505	9473
70			389	398	3743		495	530	9954
80			390	400	4105		494	554	9233
90			391	399	4634		495	586	10,308
100	404				5164	610			9498

801

802

803

804

805

806

807

808

809 **Table 3.** Equimolar excess enthalpies and excess Gibbs energies at T D 494 K in J·mol<sup>-1</sup>

810

	Excess entalpy	Excess Gibbs energy
Liquid*	-525	-350
Liquid–solid	-3360	-2072
Solid	2835	1722

811 Note: \*data derived by Ref. [70].

812

813

814

815

816

817

818

819 **Table 4.** Survey of the outcome of the analysis; numbers between parentheses are input  
820 data.

	$A$ (J·mol <sup>-1</sup> )	$B$	$\theta$ (K)	$T_c$ (K)
Minimum 494 K + Equation (5)	14,250	(0.1)	920	(448)
Thermochemical data	11,340	(0.1)	1258	448

821

822

823

824

825

826

827

828



829 **Figures Captions**

830 **Figure 1.** NaNO<sub>3</sub> and KNO<sub>3</sub> polymorphic and isostructural relationships. \*b-KNO<sub>3</sub> to  $\alpha$ -  
831 KNO<sub>3</sub> transition is reversible only for a temperature range of 400-397 K. aThe  $\beta$ -KNO<sub>3</sub> to  
832  $\gamma$ -KNO<sub>3</sub> transition temperature depends on many factors. See Ref. [7] for more information.  
833 Notes: ‘\*’ makes reference to R-3m to Pnma transition of potassium nitrate. ‘a’ makes  
834 reference to R-3m to R3m transition of potassium nitrate.

835 **Figure 2.** N-O stretching ( $\nu_1$ ) Raman band intensities (left) and position (right) for NaNO<sub>3</sub>  
836 (squares) and KNO<sub>3</sub> (crosses).

837 **Figure 3.** Powder X-ray diffraction as a function of temperature for the equimolar  
838 composition. Between temperatures of 301 and 373 K, II-NaNO<sub>3</sub> (squares) and  $\alpha$ -KNO<sub>3</sub>  
839 (crosses) coexist. At 393 K, new peaks appear: arrows point to the  $\alpha$ -KNO<sub>3</sub>  $\rightarrow$   $\beta$ -KNO<sub>3</sub>  
840 transition. Encircled peaks indicate the phase, which appears at 483 K.

841 **Figure 4.** Integral width of diffraction peaks as a function of annealing time for 20 KNO<sub>3</sub>  
842 at 483 K. Figure shows II-NaNO<sub>3</sub> (squares) and  $\beta$ -KNO<sub>3</sub> (circles).

843 **Figure 5.** X-ray powder patterns as a function of the composition after 48 h of annealing at:  
844 (a) 403 K; (b) 433 K; (c) 453 K and (d) 483 K.

845 **Figure 6.** The evolution of cell parameters as a function of composition at 483 K. a cell  
846 parameter: square marks; c cell parameter: stars. (c parameter in NaNO<sub>3</sub> is halved).

847 **Figure 7** NaNO<sub>3</sub>-KNO<sub>3</sub> phase diagram. Points: experimental DSC temperatures; plus sign:  
848  $\beta$ -KNO<sub>3</sub> solid solution type; squares: II-NaNO<sub>3</sub> solid solution type. Experimental XRD  
849 points are only depicted in the vicinity of the solvus line.

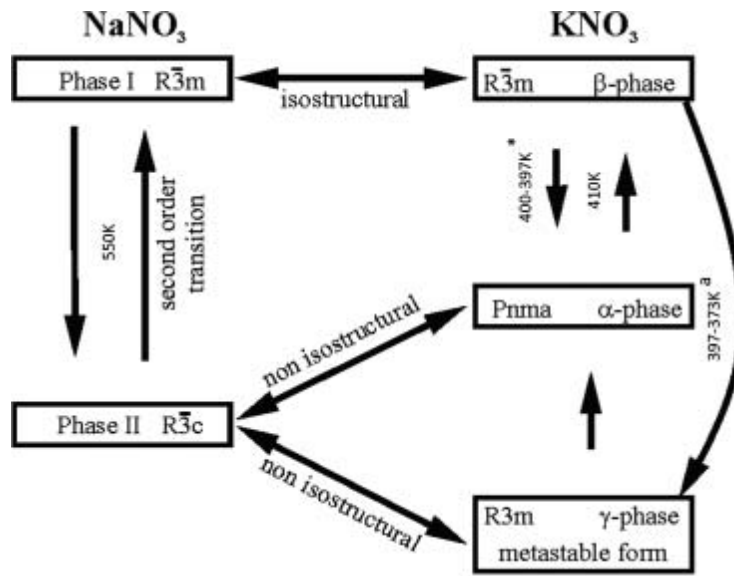
850 **Figure 8.** Calculated phase diagram using the AB $\theta$  model.

851

852

853 **Figure 1**

854



855

856

857

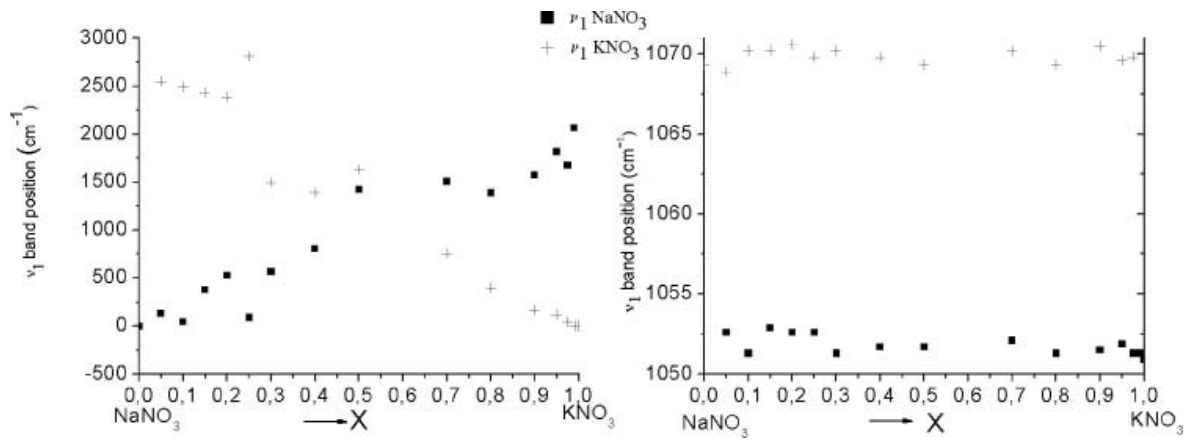
858

859

860

861 **Figure 2**

862



863

864

865

866

867

868

869

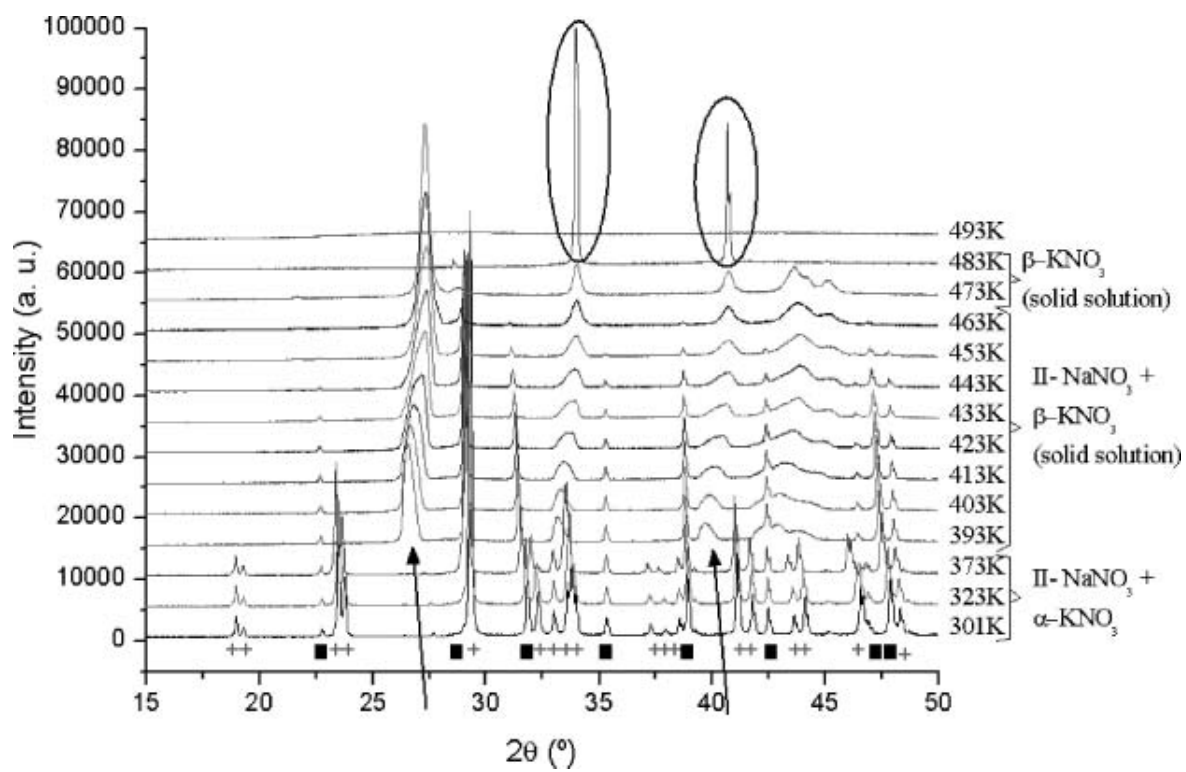
870

871

872

873 **Figure 3**

874



875

876

877

878

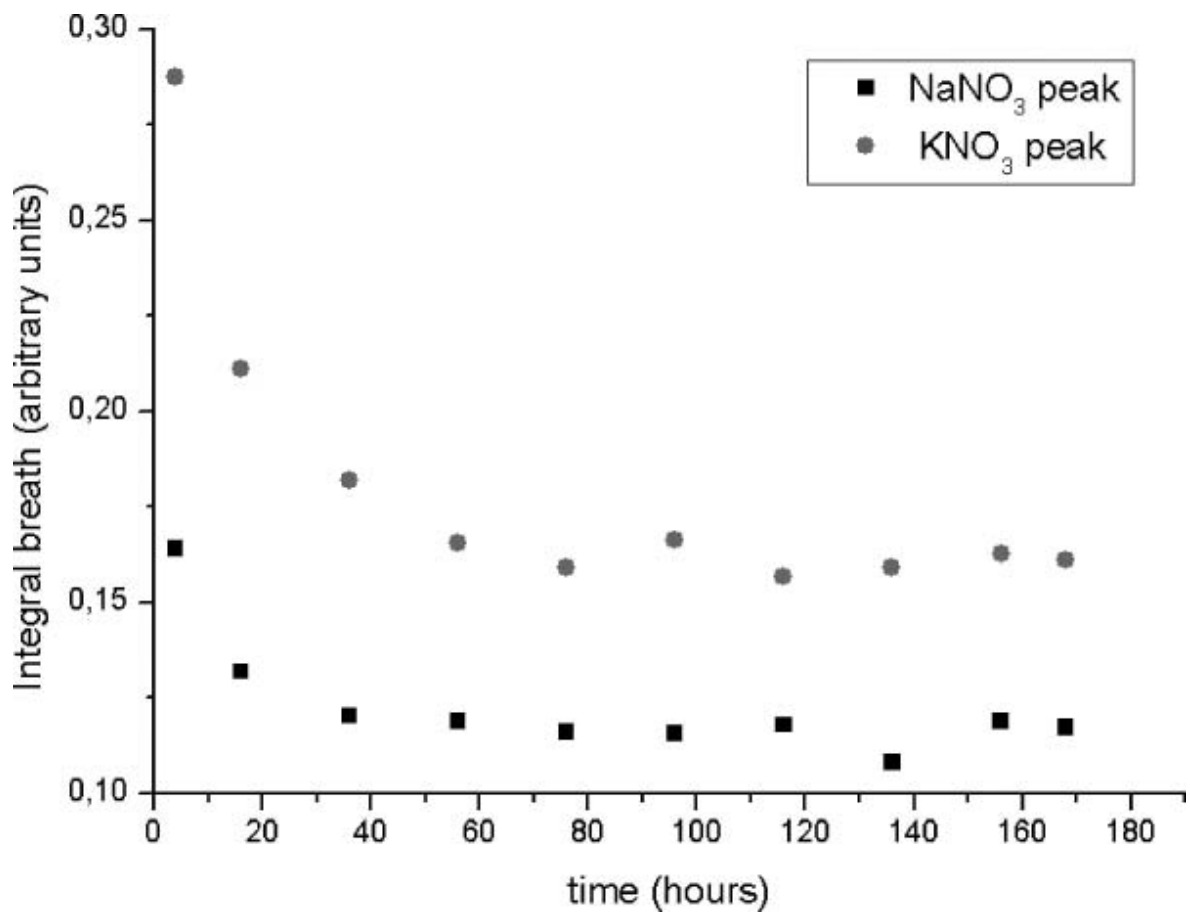
879

880

881

882 **Figure 4**

883



884

885

886

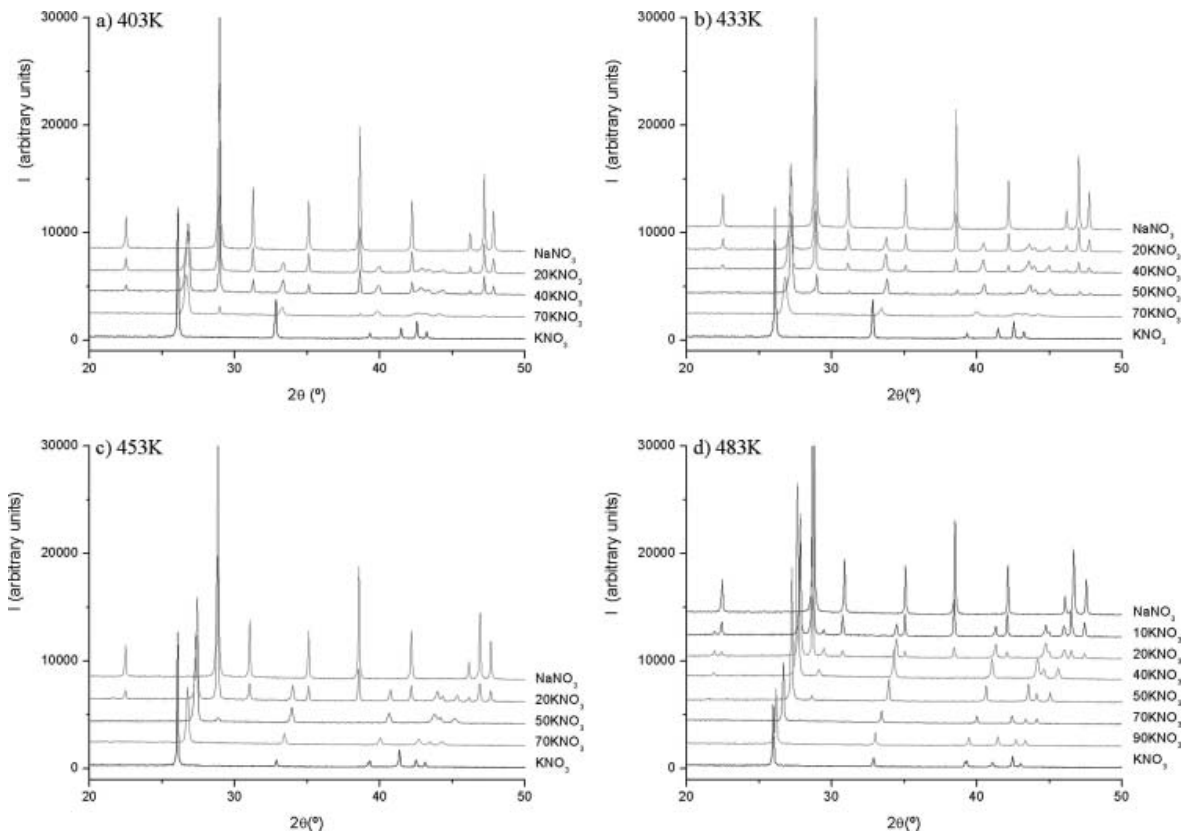
887

888

889

890 **Figure 5**

891



892

893

894

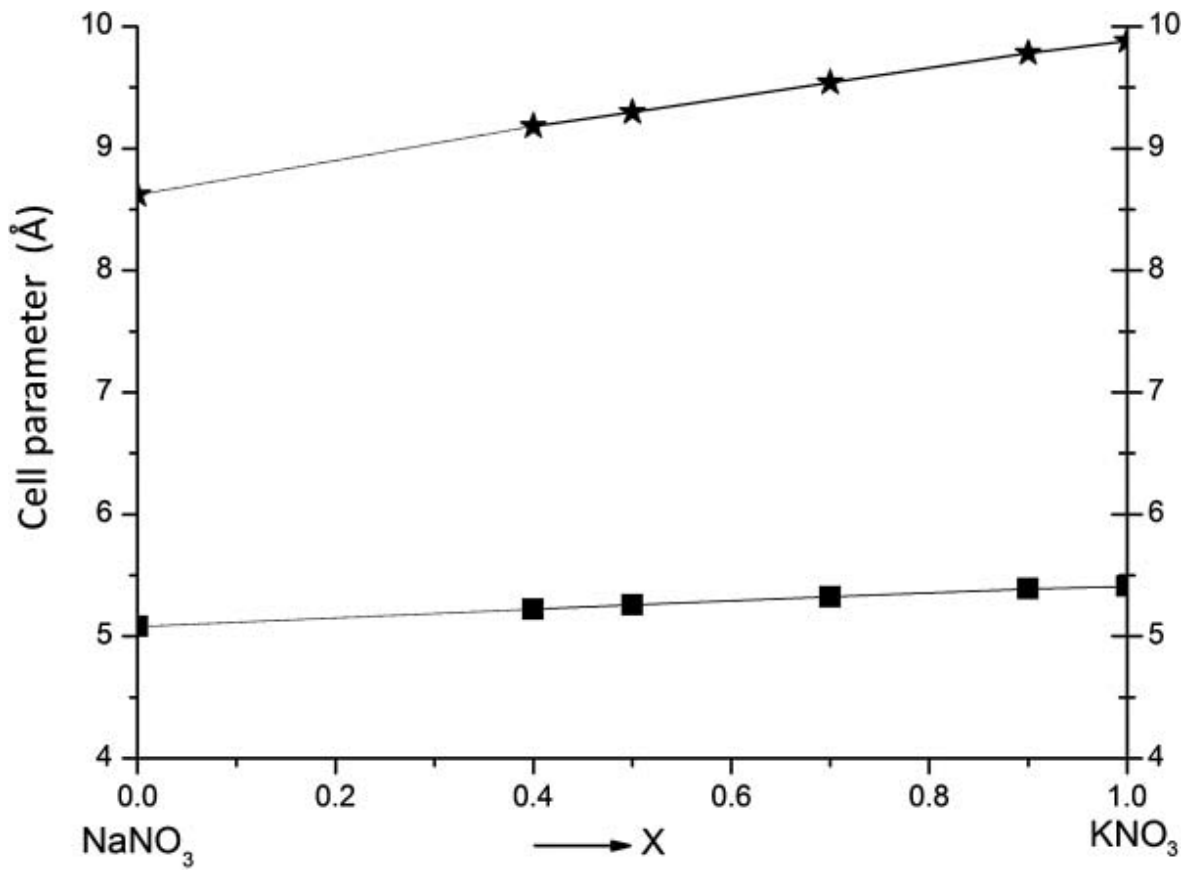
895

896

897

898 **Figure 6**

899



900

901

902

903

904

905

906

907

908

909

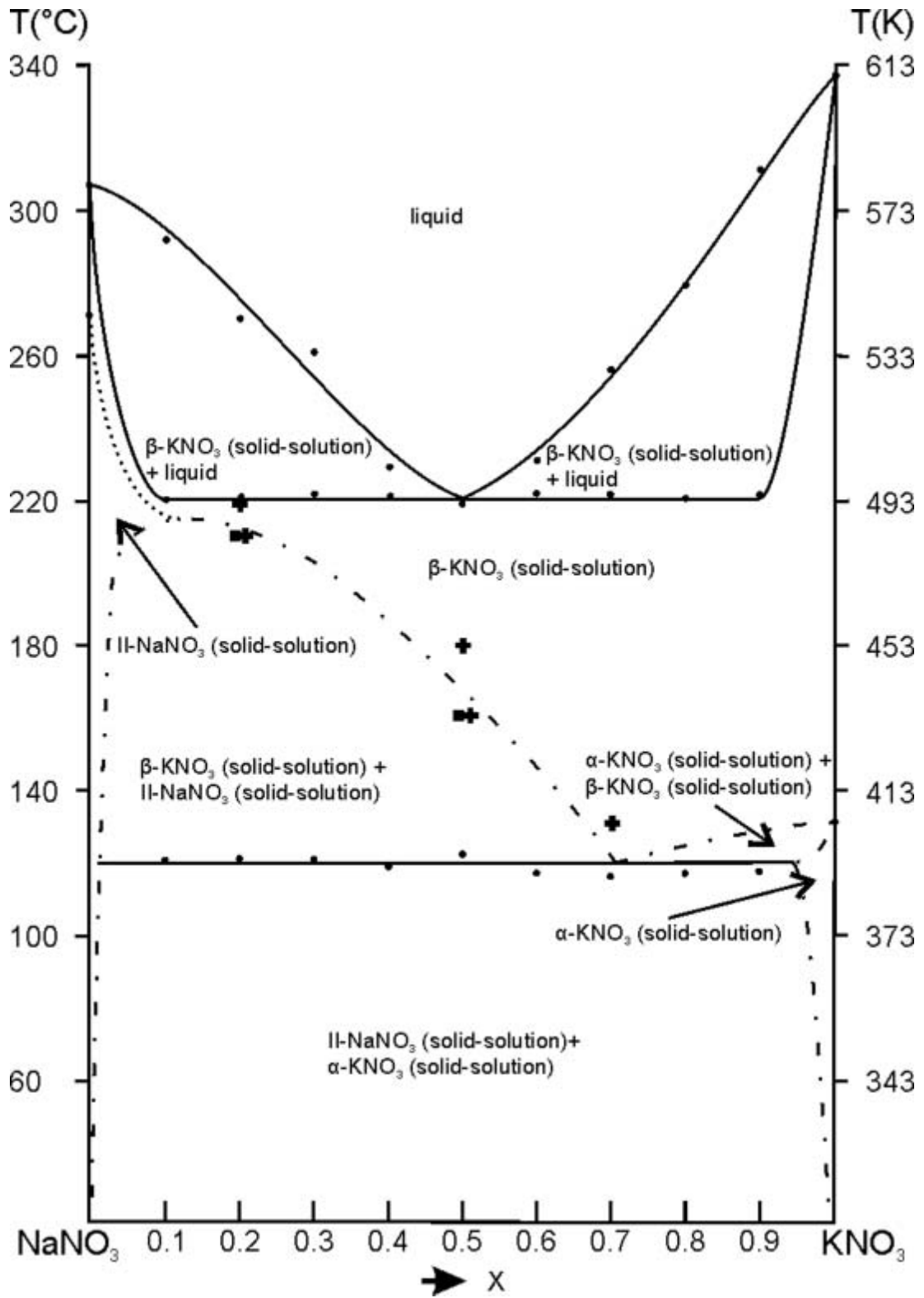
910

911

912

913 **Figure 7**

914



915

916

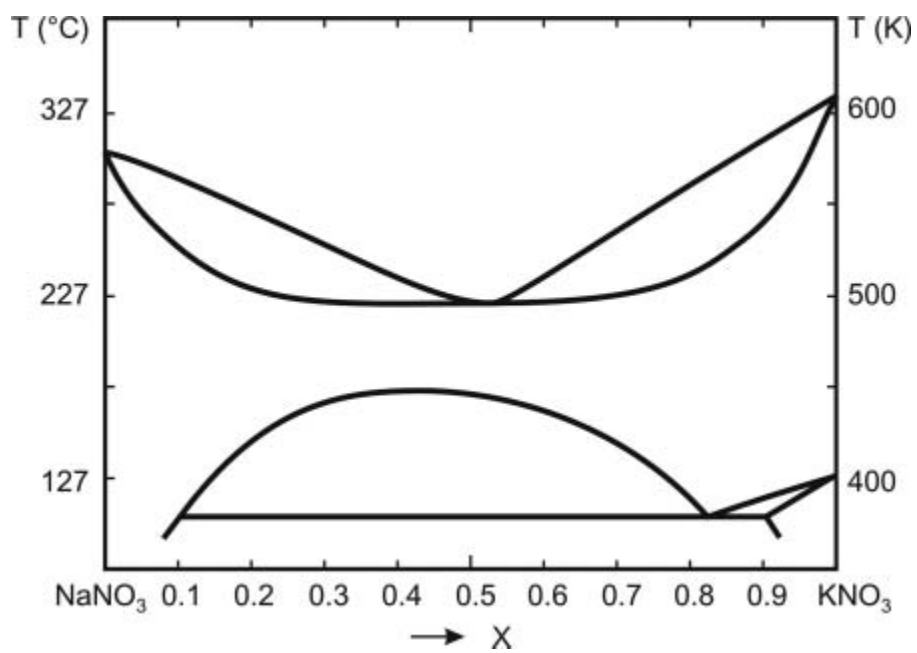
917

918



919 **Figure 8**

920



921

922

923

924

925

926